ELSEVIER

Thermochimica Acta 348 (2000) 161–168

thermochimica acta

www.elsevier.com/locate/tca

Effect of sample thickness in TMDSC measurements

Frédéric U. Buehler, James C. Seferis*

Polymeric Composites Laboratory, University of Washington, Seattle, WA 98195-1750, USA

Received 15 December 1999; received in revised form 16 December 1999; accepted 16 December 1999

Abstract

In a previous study, a mathematical model of heat diffusion in a temperature modulated differential scanning calorimetry (TMDSC) specimen was derived. The model considered the specimen to be of cylindrical geometry with top and side surfaces exposed to the block temperature while the bottom surface was considered insulated. Contrary to most other derivations found in literature, this specific model took into account both radial and axial thermal gradients within the specimen and did not neglect the thermal diffusivity of the sample. Previous numerical simulations with this model showed that temperature gradients of as much as 0.15 K can exist within a polymeric sample subjected to typical TMDSC conditions. In continuation of this work, the present investigation concentrated on assessing the effect of sample thickness on thermal gradients and time to steady-state. It also explored the influence of sample thickness on heat flow phase, without using a complex heat capacity of doubtful physical meaning. © 2000 Elsevier Science B.V. All rights reserved.

Keywords: TMDSC modeling; Temperature gradients; Thermal conductivity; Thermal diffusivity; Sample thickness

1. Introduction

In the early 1990s, traditional DSC performance was improved by the invention of temperature modulated differential scanning calorimetry (TMDSC) [1–3]. The principle of TMDSC, which must be credited to Mike Reading, consists of superimposing a sinusoidal signal over the traditional DSC heating ramp [1–3]. Advantages of this technique include the possibility of deconvoluting reversing from non-reversing signals, as well as the direct determination of heat capacity by one single run [1–3]. Since its commencement in 1993, TMDSC literature has been expanding at a very fast rate, and the interested reader is invited to consult the literature summary compiled by Menczel and Judovicts [4]. Despite this abundance of literature in diverse areas, questions still remain unanswered regarding the basic theory behind TMDSC.

One of the most controversial points in TMDSC is the existence of an imaginary heat capacity c_p''. This quantity was first suggested by Reading et al. in the case of TMDSC [2], although such a quantity had been previously reported in the case of ac-calorimetry [5]. This quantity arises from the phase angle between the in-phase and out-of-phase signals, and has been often named 'loss heat capacity' by analogy to dielectric analysis (DEA) and dynamic mechanical analysis (DMA) [6]. While it is now established that the term 'loss heat capacity' is inadequate since no heat is lost in TMDSC [7], questions remain open regarding the interpretation of the imaginary heat capacity. Every author seems to have their own personal idea on this matter, and Table 1 is only an attempt to capture the

* Corresponding author. Tel.: +1-206-543-9371; fax: +1-206-543-8386.

PII: S0040-6031(00)00351-8

Table 1
Interpretation of the imaginary part of the heat capacity according to various authors

Origin of c_p''	Reference
Time-dependent processes	[6]
Kinetic associate with the sample response	[7]
Kinetic processes within sample (crystallization, melting, relaxation)	
Dissipation processes related to entropy production	[8]
Dissipation phenomena	[9]
Work of dissipation, entropy production	[10]
Changes in molecular mobility	[11]
Entropy increase of the reservoir during one modulation cycle	[12]
Energy transfer between external and internal degrees of freedom	[13]
Dissipated energy of the driving force of the time-dependent processes	[14]
Mathematical artifact	[15]

variety of explanations that have been proposed so far regarding the origin of c_p'' [6–15]. The confusion around c_p'' finds its roots in the mathematical modeling that is traditionally used for TMDSC. Most traditional models consider the sample temperature to be uniform at any time [1,2,9,16]. This corresponds to asserting that the sample's heat conductivity is infinite, or at least extremely large. This is of course rarely the case, perhaps with the exception of metallic samples. Therefore, a complete TMDSC model should include thermal conductivity and take into account thermal gradients within the sample. The importance of thermal gradients within a similar crucible and experimental set-up had already been realized as early as 1969 by Wilburn and co-workers in the case of differential thermal analysis (DTA) [17–19]. Their model included radial gradients only, and of course had different boundary conditions since DTA is not a modulated technique. In 1994, Marcus and Blaine reported being able to determine thermal conductivity of various substances by TMDSC [20], but did not provide an accurate description of their model until 4 years later [21]. In the meantime, several authors started to develop models which included thermal conductivity. The first noticeable attempt was realized by Lacey et al. in 1997 [16]. Unfortunately, these authors lumped thermal conductivity into some kind of calibration factor, and did not specify the sample geometry. That same year, Schenker and Stäger proposed a model which took into account sample geometry, but considered axial gradients only [22]. Their model was very similar to one developed concurrently by Simon et al. to calculate thermal conductivity from TMDSC [23–24]. In 1998, Buehler et al. proposed a model of heat transfer within a TMDSC sample where not only axial temperature gradients were accounted for, but also radial temperature gradients [15]. Their model was used to investigate the temperature transient behavior at early times, the temperature profiles throughout the specimens, and the heat flow phase dependence on thermal conductivity [25]. However, these investigations were carried out for a specimen of specific radius to height ratio, and the contributions of sample thickness were left unexplored.

As a continuation of this work, the objective of the present paper is to examine the influence of sample thickness in TMDSC experiments. First, sample thickness effect on the time to reach quasi-steady-state was examined. Second, thickness effect on both axial and radial temperature gradients was assessed. And third, thickness influence on phase lag was established.

2. Theory

The model used in this work is based on earlier developments [15,25]. The DSC sample was considered as a right cylinder of radius R and of variable thickness L, as shown in Fig. 1. Temperature was considered to be a function of axial position z, radial position r, and time t [15]. The heat diffusion equation:

$$\frac{\partial T}{\partial t} = \alpha \nabla^2 T \tag{1}$$

was expressed in cylindrical co-ordinates, and associated with the following boundary conditions [15]:

$$T(r, z, 0) = T_o \tag{2}$$

$$T(R, z, t) = T_b \tag{3}$$

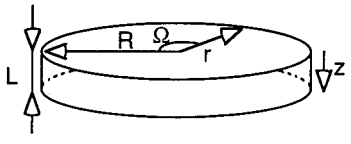

Fig. 1. DSC sample is modeled as a right cylinder of radius R and of various thickness L.

$$T(r,0,t) = T_b \tag{4}$$

$$-k\frac{\partial T}{\partial z}(r,L,t) = 0 \tag{5}$$

$$\frac{\partial T}{\partial r}(0,z,t) = 0 \tag{6}$$

where α is equal to thermal diffusivity (m^2/s); k to thermal conductivity (W/m K); T_o initial sample temperature (K) and T_b furnace (block) temperature (K) is equal to $T_{bo}+bt+A\sin(\omega t)$.

To solve Eq. (1), appropriate changes of variables were carried out to convert the boundary conditions from inhomogeneous to homogeneous. As a result of this operation, the heat diffusion equation became a Sturm–Liouville problem with a source term, which was solved by the use of Green's functions. A detailed development of the procedure is available elsewhere [15]. Finally, the solution was converted back into its original variables and the heating rate b was set to zero because the quasi-isothermal case was studied. This provided:

$$T(r,z,t) = \sum_{p=1}^{\infty}\sum_{n=1}^{\infty}\left\{\left[E_{n,p} - \frac{A\omega R^2}{\Lambda'_{n,p}}\sin(\omega t) - \frac{A\omega R^2}{\Lambda''_{n,p}} \times \cos(\omega t)\right] J_o\left(\lambda_n \frac{r}{R}\right)\sin\left(\mu_p \frac{z}{L}\right)\right\} + T_b \tag{7}$$

where

$$E_{n,p} = \frac{4}{\mu_p \lambda_n J_1(\lambda_n)}\left(e^{-((\kappa_{n,p}^2 \alpha t)/R^2)}\right) \times \left(T_o - T_{bo} + \frac{A\omega R^2 \kappa_{n,p}^2}{\alpha(\kappa_{n,p}^4 + (R^4\omega^2/\alpha^2))}\right) \tag{8}$$

$$\frac{1}{\Lambda'_{n,p}} = \frac{4}{\mu_p \lambda_n J_1(\lambda_n)}\left[\frac{\omega R^2}{\left(\kappa_{n,p}^4 \alpha^2 + \omega^2 R^4\right)}\right] \tag{9}$$

$$\frac{1}{\Lambda''_{n,p}} = \frac{4\kappa_{n,p}^2}{\mu_p \lambda_n J_1(\lambda_n)}\left[\frac{\alpha}{\left(\kappa_{n,p}^4 \alpha^2 + \omega^2 R^4\right)}\right] \tag{10}$$

λ's satisfy the transcendental equation

$$J_o(\lambda_n) = 0 \tag{11}$$

$$\mu_p = (2p-1)\frac{\pi}{2} \tag{12}$$

where p is an integer

$$\kappa_{n,p}^2 = -\left(\lambda_n^2 + \frac{R^2}{L^2}\mu_p^2\right) \tag{13}$$

The $E_{n,p}$ terms represent the exponential decay (transient) part of the solution, which vanishes at sufficiently long times. Note that these terms depend on the thickness L of the sample through the Eigenvalue $\kappa_{n,p}$. The remaining terms in the square bracket of Eq. (7) represent the quasi-steady-state (asymptotic) solution. These terms also depend on the thickness L of the sample through $\kappa_{n,p}$.

Because most TMDSC cells have the measuring thermocouples located at the center bottom of the specimen, r and z could be set to zero and L, respectively. Eq. (7) was then simplified to:

$$T(0,L,t) = \left[E - \frac{A\omega R^2}{\Lambda'}\sin(\omega t) - \frac{A\omega R^2}{\Lambda''}\cos(\omega t)\right] + T_b \tag{14}$$

with

$$E = \sum_{n=1}^{\infty}\sum_{p=1}^{\infty}(-1)^{p+1}E_{n,p} \tag{15}$$

$$\frac{1}{\Lambda'} = \sum_{n=1}^{\infty}\sum_{p=1}^{\infty}(-1)^{p+1}\frac{1}{\Lambda'_{n,p}} \tag{16}$$

$$\frac{1}{\Lambda''} = \sum_{n=1}^{\infty}\sum_{p=1}^{\infty}(-1)^{p+1}\frac{1}{\Lambda''_{n,p}} \tag{17}$$

where Λ' and Λ'' are the effective thermal diffusivities defined previously in ref. [15], with a slight correction to ensure that they are alternating series. With this more manipulatable form of Eq. (7), time to quasi-steady-state and phase quantities were easily determined. Time to quasi-steady-state was defined as the time needed for all the transient solution E to contribute to less than 5×10^{-3} K to the asymptotic solution. Mathematically, this gives:

$$t_{ss} = \text{time at which } E = 5\times10^{-3}\text{K} \tag{18}$$

Because it is convenient to work with dimensionless quantities, the number of modulation periods to quasi-steady-state, n_{ss}, was defined:

$$n_{ss} = t_{ss}\frac{\omega}{2\pi} \tag{19}$$

The phase angle φ, defined as the phase between the specimen temperature and the block temperature, was calculated with:

$$\varphi = \arctan\left(-\frac{A - A\omega R^2(1/\Lambda')}{A\omega R^2(1/\Lambda'')}\right) \quad (20)$$

while the heat flow phase γ, which is the phase angle between the derivative of temperature and the heat flow, was calculated with [21]:

$$\gamma = \pi - \arctan\left(\frac{(1/\Lambda_r'') - (1/\Lambda_s'')}{(1/\Lambda_r') - (1/\Lambda_s')}\right) \quad (21)$$

The above equation is valid for an ideal cell (no cell contribution to phase lag).

Temperature profiles along the axial and radial co-ordinates had to be determined from Eq. (7). To simplify calculations, time t was chosen as greater than t_{ss}, allowing the transient terms to be neglected. For axial temperature profiles, the r co-ordinate was chosen as r=0 to yield:

$$T(0, z, t > t_{ss}) = \sum_{p=1}^{\infty}\sum_{n=1}^{\infty}\left\{\left[-\frac{A\omega R^2}{\Lambda'_{n,p}}\sin(\omega t) - \frac{A\omega R^2}{\Lambda''_{n,p}}\cos(\omega t)\right]\sin\left(\mu_p\frac{z}{L}\right)\right\} + T_b \quad (22)$$

In the case of radial temperature profiles, the z co-ordinate was set to L to yield:

$$T(r, L, t > t_{ss}) = \sum_{p=1}^{\infty}\sum_{n=1}^{\infty}\left\{\left[-\frac{A\omega R^2}{\Lambda'_{n,p}}\sin(\omega t) - \frac{A\omega R^2}{\Lambda''_{n,p}}\cos(\omega t)\right]J_o\left(\lambda_n\frac{r}{R}\right)\sin(\mu_p)\right\} + T_b \quad (23)$$

3. Numerical

Numerical simulation of the specimen temperature evolution and profile were carried out under quasi-isothermal conditions for an aluminum reference pan and a polyethylene terephthalate (PET) sample using the equations developed above with 20 Eigenvalues for each Eigenvector [15]. The modulation amplitude was set to 0.5 K every 60 s at the quasi-isothermal temperature of 293 K, while the specimen radius over height ratio (R/L) was allowed to vary between 1.5 and 100 for most calculations. Table 2 summarizes the parameters used for the simulation.

Table 2
Parameters used for the numerical simulation with typical values

Parameter	Symbol	Value	Units
Modulation amplitude	A	0.5	K
Radius of the specimen	R	3.3	mm
Height of specimen	L	$0.033 \leq L \leq 2.2$	mm
Initial temperature of the sample	T_0	293	K
Isothermal experiment	b	0	K/s
Aluminum pan	α_r	9.71×10^{-5}	m^2/s
PET sample	α_s	0.93×10^{-7}	m^2/s
Modulation period of 60 s	ω	$2\pi/60$	rad/s

Time to quasi-steady-state was determined by calculating $T(0, L, t)$ from Eq. (14) with and without term E for 100 points equally spaced in time between t=0 and t=120 s. As soon as E contributed to less than 0.005 K, the corresponding time was set as t_{ss} and n_{ss} was calculated through Eq. (19). Calculations were repeated for seven different R/L ratios of 0.1, 1, 1.5, 3, 4.459, 10, 100. The ratio of 4.459 corresponds to the typical R/L ratio as defined in references [15,25].

Axial and radial profiles were calculated from Eqs. (22) and (23), respectively. Time was set to 60 s, and 50 co-ordinate points were chosen between the values of zero and L, zero and R, respectively. Calculation were carried out both for aluminum and PET specimens, and repeated for the R/L ratios of 1.5, 3, 4.459, 10, and 100.

Phase calculations were carried out according to Eqs. (20) and (21) for 25 logarithmically spaced α_s/α_r spread over four decades from 0.0001 to 1. Time was set to 60 s, and calculations were repeated for the five R/L ratios of the temperature profile determination.

4. Results

First, the time taken for the reference and sample to reach quasi-steady-state was investigated. It was found that the aluminum reference reached a quasi-steady-state almost immediately (<1.2 s), regardless of its radius to height ratio. On the other hand, the PET

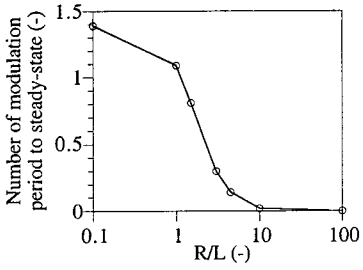

Fig. 2. Time to quasi-steady-state for a PET sample of various *R*/*L* ratio.

sample under investigation showed a great dependence upon the sample geometry. Fig. 2 shows that thin PET samples having a radius to height ratio of 10 or more reached quasi-steady-state very rapidly. However, thicker samples had an appreciable temperature transient, and in the case of very thick PET samples (R/L=0.1), the time to quasi-steady-state was more than one and a half times the period of amplitude modulation. Such thick samples are never found in practice, and were included here only to test the robustness of the model. In real TMDSC experiments, *R*/*L* ratios of less than 1.5 are rarely encountered, and from now on simulations are to be limited to ratios between 1.5 and 100.

Fig. 3 shows the temperature profile along the *z*-axis of the cylindrical specimen for the aluminum reference pan and the PET sample. This is a 'snapshot' of the temperature profile at an arbitrary time t=60 s once pseudo-steady-state was reached. For both specimens, the axial temperature gradients were negligible for $R/L \geq 100$. Which means that very thin specimens can be considered isothermal along their height. As the thickness of the specimen increased and *R*/*L* decreased, thermal gradients started to appear and became more and more important. In the case of the PET sample, which has a much lower thermal diffusivity than the aluminum reference, increase in thickness had a much more drastic effect on the axial thermal gradient increase. Indeed, as seen on Fig. 3b, a PET sample with R/L=1.5 can have an axial thermal gradient of 0.32 K. An aluminum reference of identical geometry displayed a thermal gradient of only 0.85 mK — more than three orders of magnitude less.

The proposed model did not only take into account axial temperature gradients, it also considered radial gradients. These are displayed in Fig. 4, which shows a 'snapshot' of the *r*-axis temperature across the bottom face of a specimen. Thin aluminum reference pans ($100 \geq R/L \geq 10$) did not exhibit radial thermal gradients, while thicker reference pans were found to have thermal gradients in the order of one thousandth of a Kelvin (R/L=1.5, Fig. 4a). As observed earlier for the axial gradients, polymeric samples had higher temperature gradients due to their lower thermal diffusivity. For the case of PET, Fig. 4b shows that radial thermal gradients can reach several tenths of a Kelvin for thick samples (R/L=1.5).

Another issue in TMDSC is the phase angle, or phase lag. In previous papers [15,25], we defined two phase angles: φ, which is the phase angle between the specimen's response and the block temperature, and ψ, which is the phase angle between the cyclic part of the temperature difference ($T_s - T_r$) and the block temperature (T_b). Very often the phase angle reported in literature is the heat flow phase, which is frequently referred to simply as 'phase lag' [3,8,26]. This phase

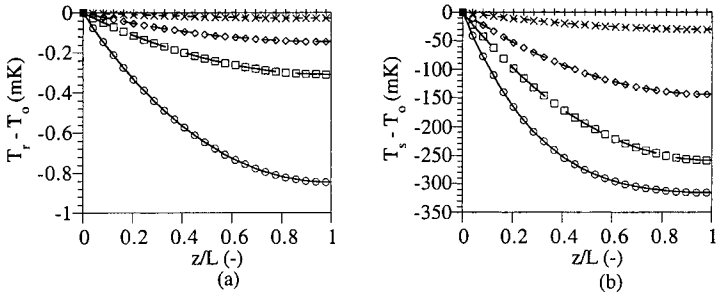

Fig. 3. Temperature profile along the *z*-axis of (a) an Aluminum reference and (b) a PET sample for various *R*/*L* ratios. R/L=100(+), 10(×), 4.459(◇), 3(□), 1.5(○).

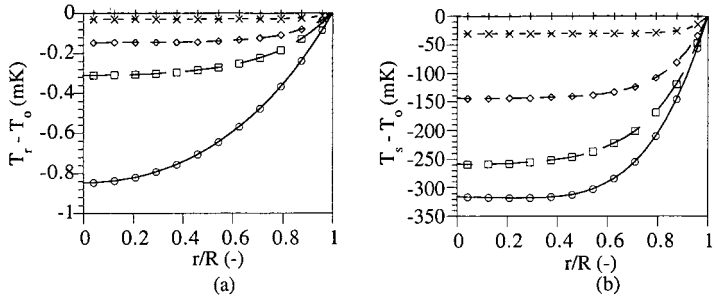

Fig. 4. Temperature profile along the *r*-axis of (a) an aluminum reference and (b) a PET sample for various *R*/*L* ratios. *R*/*L*=100(+), 10(×), 4.459(◇), 3(□), 1.5(○).

lag corresponds to the phase angle between the derivative of temperature and the heat flow, and has been denoted as γ in our previous paper [25].

Provided there is no instrumental contribution to phase lag, γ and ψ are supplementary angles, i.e., $\gamma=180-\psi$ [25]. Fig. 5 shows φ_s and γ for various *R*/*L* ratios based on the ratio between sample thermal diffusivity and reference (aluminum) thermal diffusivity. It was established earlier that the phase angles were dependent upon the sample thermal diffusivity [15]. Now, as demonstrated in Fig. 5, the sample geometry was also found to have an influence. This is because the phase lag depends not only on the thermal diffusivity, but also on the length of diffusion path, i.e. the height and radius of the specimen. Thin samples (*R*/*L*=100), which were seen earlier not to show any significant temperature gradients along either axis, were found to have a 90° phase lag regardless of their thermal diffusivity. This was explained by the very short path of diffusion that existed in these samples between their top and bottom surface. Even with a very low thermal diffusivity, the path being so short, no phase lag was observed. Conversely, samples of high thermal diffusivity were found to be less affected by geometry as heat could diffuse efficiently even for long paths. This was especially true for samples which had a thermal diffusivity higher than a tenth of that of aluminum ($\alpha_s/\alpha_r=0.1$). Note that most thermoplastic and composite materials have their thermal diffusivity between 0.001 and 0.003 times that of aluminum [15], where the sample geometry is then of importance. These observations might explain some of the variation reported by Reading and Luyt in phase lag between samples of various weight [26]. These authors noticed that the phase lag changed with sample weight and carrier gas, but were not able to give a satisfying explanation as why it was so [26]. Now it is clear that an increase in sample weight, provided that it results in a thicker sample, will have a higher phase

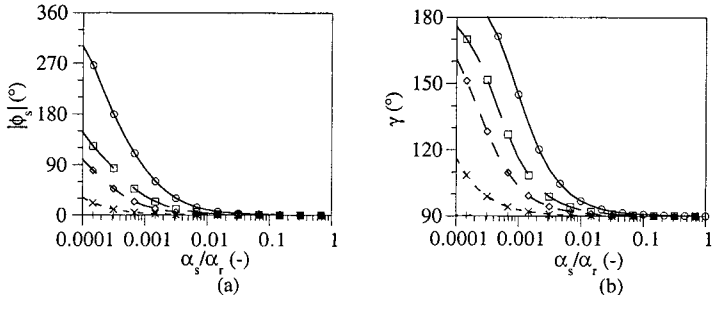

Fig. 5. Dependence of the (a) sample phase angle and (b) sample phase lag on thermal diffusivity and geometry. *R*/*L*=100(+), 10(×), 4.459(◇), 3(□), 1.5(○).

lag. Concerning the effect of the gas carrier, further investigations are needed to include the gas heat transfer coefficient in the model.

5. Conclusions

In this study, a previous mathematical model of heat diffusion in a TMDSC specimen was modified to study the importance of sample thickness. The model considered the specimen to be a cylinder of varying geometry with a radius to height ratio comprised between 1.5 and 100. Top and side surfaces of the specimen were considered to follow the furnace temperature, while the bottom surface was considered insulated. Numerical simulations showed that very thin polymeric samples (R/L=100) reached quasi-steady-state almost instantaneously, had negligible temperature gradients, and had practically no phase lag. On the other hand, thick polymeric samples (R/L=1.5) were found to reach quasi-steady-state after 0.8 modulation periods. Such samples displayed thermal gradients of 0.3 K, both in the axial and radial directions. Moreover, in the case of polymeric samples, phase lag was found to be dependent upon sample's thickness, and thicker samples were found to have some significant phase lag. Collectively, this study showed that unless TMDSC samples are as thin as 33 μm, thermal gradients will prevail in polymeric samples. Therefore, these gradients should be accounted for when deconvoluting the reversing and non-reversing signals to avoid the use of a complex heat capacity of questionable physical meaning.

6. Nomenclature

Latin letters

A	modulation amplitude (K)
b	linear heating rate (K s)
c_p	specific heat capacity as defined thermodynamically (J kg K)
c'_p	in-phase component of the specific heat capacity (J kg K)
c''_p	out-of-phase component of the specific heat capacity (J kg K)
E	exponential decay (transient) part of the heat transfer solution (K)
k	thermal conductivity (W/m K)
L	specimen height (m)
r	radial co-ordinate (m)
R	specimen radius (m)
t	time (s)
T	temperature (K)
z	axial co-ordinate (m)

Indices

b	block (furnace)
n	index of the radial eigenvalues
o	initial
p	index of the axial eigenvalues
r	reference
s	sample
ss	steady-state

Greek letters

α	thermal diffusivity (m^2/s)
γ	Phase angle between the derivature of temperature and heat flow (rad)
$\kappa_{n,p}$	Eigenvalues depending on the sample geometry (−)
λ_n	Eigenvalue related to the radial position (−)
μ_p	Eigenvalue related to axial position (−)
φ	phase angle between the specimen response and the block temperature (rad)
ψ	phase angle between the cyclic part of the temperature difference and the block temperature (rad)
ω	pulsation of the oscillation (rad/s)
Λ'	effective thermal diffusivity term that arises in the in-phase component of the specimen temperature (m^2/s)
Λ''	effective thermal diffusivity term that arises in the out-of-phase component of the specimen temperature (m^2/s)

Acknowledgements

The authors express their appreciation to T.A. Instruments for continuous support to the Polymeric Composites Laboratory at the University of Washington. Support for this work was also provided by The Boeing Company through the Boeing-Steiner professorship.

References

[1] M. Reading, D. Elliott, V.L. Hill, J. Thermal Anal. 40 (1993) 949.
[2] M. Reading, R. Wilson, H.M. Pollock, in: Proceedings of the 23rd Conference of the NATAS, Toronto, 1994, 2.
[3] P.S. Gill, S.R. Sauerbrunn, M. Reading, J. Thermal Anal. 40 (1993) 931.
[4] J.D. Menczel, L. Judovits, J. Thermal Anal. 54 (1998) 419.
[5] N.O. Birge, S.R. Nagel, Phys. Rev. Lett. 54 (1985) 2674.
[6] J.E.K. Schawe, Thermochimica Acta 260 (1995) 1.
[7] M. Reading, J. Thermal Anal. 54 (1998) 411.
[8] S.R. Aubuchon, P.S. Gill, J. Thermal Anal. 49 (1997) 1039.
[9] J.E.K. Schawe, Thermochimica Acta 271 (1996) 127.
[10] J.E.K. Schawe, G.W.H. Höhne, Thermochimica Acta 287 (1996) 213.
[11] J.E.K. Schawe, G.W.H. Höhne, J. Thermal Anal. 46 (1996) 893.
[12] Y.-H. Jeong, Thermochimica Acta 304/305 (1997) 67.
[13] I. Alig, Thermochimica Acta 304/305 (1997) 35.
[14] G.W.H. Höhne, Thermochimica Acta 304/305 (1997) 121.
[15] F.U. Buehler, C.J. Martin, J.C. Seferis, J. Thermal Anal. 54 (1998) 501.
[16] A.A. Lacey, C. Nikopoulos, M. Reading, J. Thermal Anal. 50 (1997) 279.
[17] R. Melling, F.W. Wilburn, R.M. McIntosh, Anal. Chem. 41 (1969) 1275.
[18] F.W. Wilburn, D. Dollimore, J.S. Crighton, Thermochimica Acta 181 (1991) 173.
[19] F.W. Wilburn, D. Dollimore, J.S. Crighton, Thermochimica Acta 181 (1991) 191.
[20] S.M. Marcus, R.L. Blaine, Thermochimica Acta 243 (1994) 231.
[21] R.L. Blaine, S.M. Marcus, J. Thermal Anal. 54 (1998) 467.
[22] B. Schenker, F. Stäger, Thermochimica Acta 304/305 (1997) 219.
[23] S.L. Simon, Macromolecules 30 (1997) 4056.
[24] S.L. Simon, J.W. Sobieski, G.B. McKenna, in: Proceedings of the 26th Conference of the North American Thermal Analysis Society, Cleveland, OH, 1998, 129.
[25] F.U. Buehler, J.C. Seferis, Thermochimica Acta 334 (1999) 49.
[26] M. Reading, R. Luyt, J. Thermal Anal. 54 (1998) 535.